Does deterministic chaos imply intermittency in fully developed turbulence?

Jens Eggers and Siegfried Grossmann
Fachbereich Physik der Philipps-Universität Renthof 6, D-3550 Marburg, Germany

(Received 21 June 1990; accepted 28 March 1991)

A Fourier–Weierstrass decomposition of the velocity field is introduced. The admitted number of real amplitudes is 572 or 836. They are determined numerically from the Navier–Stokes equation including viscosity, driven by constant energy input stirring the largest eddies only. In another calculation, the energy input is provided by an external shear. The Reynolds number Re is about 10^6, the inertial range comprises about 2 decades, and there are 11 levels of successively decaying eddies. The hierarchical mode ansatz thus allows for a state of high turbulence, which usually is inaccessible numerically. Deterministic chaos is found on all scales. The mean values of the amplitudes scale with the eddy size r as r^{ζ} with ζ very near 1/3. Expected deviations $\delta\zeta = \zeta - 1/3$, as one typical signature of intermittency, are very small only, well compatible with none at all. So, despite stochasticity (chaos) in the Fourier–Weierstrass decomposition with a tractably restricted set of plane waves, intermittency in the velocity scaling cannot be found. This changes if, in addition to temporal chaos, a spatial branching of the eddy decay process is also admitted.

I. INTRODUCTION

The Eulerian velocity field $u_i(\mathbf{x},t)$ in high Reynolds number flow is irregular both as a function of time t at fixed position and as a function of position $\mathbf{x}$ at given time. It is generally believed that this apparent stochasticity is due to the nonlinear character of the Navier–Stokes equation even without explicitly coupled external noise, although most theories do couple Gaussian noise.

Despite the deterministic chaos of probably high dimension, the flow field shows self-similarity of the mean eddy energy distribution

$$\langle\langle|\mathbf{u}(\mathbf{x}+\mathbf{r},t)-\mathbf{u}(\mathbf{x},t)|^2\rangle\rangle = b\epsilon^{2/3}r^{2/3}. \tag{1}$$

Here, $\langle\langle\cdots\rangle\rangle$ denotes the averages on t or on x or on the statistical ensemble; r is the varying eddy size, $\epsilon = \langle\langle\partial_i u_j\,\partial_i u_j\rangle\rangle$ the mean energy dissipation rate per unit mass; the numerical factor is $b = 8.4$ empirically (see, e.g., Refs. 1 and 2). Equation (1) is the prediction of the classical scaling theories by Kolmogorov,[3] Obukhov,[4] von Weizsäcker,[5] Heisenberg,[6] and Onsager[7] and holds in the inertial subrange (ISR) $9\eta \lesssim r \lesssim L$, with $\eta = (\nu^3/\epsilon)^{1/4}$ as the Kolmogorov viscous scale and L the external scale.

The present state of the art of measuring (see, for example, Refs. 8 and 1) confirms (1) or the corresponding wavenumber spectrum

$$E(k) = C\epsilon^{2/3}k^{-5/3}. \tag{2}$$

The numerical factor C corresponding to b is (cf. Ref. 1)

$$C = 5\left[9\Gamma\left(\tfrac{1}{3}\right)\right]^{-1}b = 1.74. \tag{3}$$

But in particular, the scaling exponents $\zeta(m)$ of the higher-order structure functions defined by

$$D_m(r) = \langle\langle|\mathbf{u}(\mathbf{x}+\mathbf{r},t)-\mathbf{u}(\mathbf{x},t)|^m\rangle\rangle \propto (r/L)\zeta(m) \tag{4}$$

seem to have significant departures[8] from

$$\zeta_{\rm cl} = m/3, \tag{5}$$

as found in the classical theory.[3–7] One line of reasoning (originating from Landau[9]) attributes these deviations to fluctuations in the local energy dissipation rate

$$\epsilon(\mathbf{x},t) = (\nu/2)\left[\partial_j u_i(\mathbf{x},t) - \partial_i u_j(\mathbf{x},t)\right]^2, \tag{6}$$

whose mean is ϵ. The highly spotty or "intermittent" character of $\epsilon(\mathbf{x},t)$ in space and time (e.g., Ref. 10) leads to a scaling dependence of the moments of $\epsilon(\mathbf{x},t)$ on the scale r of observation, for example,

$$\langle\langle[\epsilon(\mathbf{x},t)-\epsilon][\epsilon(\mathbf{x}+\mathbf{r},t)-\epsilon]\rangle\rangle \propto \epsilon^2(r/L)^{-\mu}. \tag{7}$$

This spottiness also shows up in the intricate structures formed by the vorticity field. Numerical simulations[11] give a vivid idea of this spatial intermittency.

Still another signature of intermittency is the Reynolds number dependence of scale-independent moments,[11–13] such as the skewness

$$S = \frac{\langle\langle(\partial_1 u_1)^3\rangle\rangle}{\langle\langle(\partial_1 u_1)^2\rangle\rangle^{3/2}} \propto \mathrm{Re}_\lambda^{\mu_S}$$

or the kurtosis

$$K = \frac{\langle\langle(\partial_1 u_1)^4\rangle\rangle}{\langle\langle(\partial_1 u_1)^2\rangle\rangle^{2}} \propto \mathrm{Re}_\lambda^{\mu_K}.$$

The ϵ exponent μ can be tied to $\zeta(m)$ by various reasonings. For example, the log-normal theory[14] says $\zeta(m) = m/3 - m(m-3)/18$. Other theories are the β model[15,16] or the statistical β model,[17] leading to slightly different relations between μ and $\zeta(m)$. According to the data, μ ranges from 0.20–0.50 depending not only on the specific measurement but also on the type of correlation function considered [either (7) or $\langle\langle\epsilon(\mathbf{x},t)\epsilon(\mathbf{x}+\mathbf{r},t)\rangle\rangle$].

Analytical theories of turbulence,[2,18,19] (and many more references therein) seem to describe many properties of turbulent flow quite accurately. In particular, the variable range decomposition[2] allows to evaluate the structure function $D(r)$ in all ranges, inertial (ISR) as well as viscous (VSR), without any free parameter and without divergen-

 0899-8213/91/081958-11$02.00

cies, in agreement with data to within about 20%. There are, as always, some basic assumptions about the statistical properties of the Navier–Stokes solutions: isotropy, homogeneity, and a mean-field-like decoupling of the sub-r- and super-r-scales.

An accepted theory of intermittency, based on the Navier–Stokes equation, is still missing. There are models (as quoted above) but no convincing analytical proof of the existence of intermittency and of its mechanism. While analysis of data seems to confirm it, as just mentioned and as also found in a recent wavelet analysis of a long turbulent flow signal,[20] the perturbation theory by Belinicher and L'vov[21] seems to prove the nonexistence of intermittency.

In a recent paper,[22] Kraichnan also raised doubts on the fractal properties of turbulent flow and on intermittency corrections $\delta\zeta(m)$, based on a theory for the probability distribution function for the velocity field.

We attack this question of fundamental interest in this paper by introducing a limited and thus tractable number of modes into the Navier–Stokes equation. We take care of the self-similarity by defining a Fourier–Weierstrass decomposition of the flow field. The Lagrangian, Galilean invariant character is preserved as far as necessary. The mode decomposition in terms of $\exp(i\mathbf{p}\cdot\mathbf{x})$ respects the possibility of spatial isotropy. No explicit boundaries are introduced; the largest scale is present by the size $2\pi L$ of the periodicity box. The mode amplitudes are determined by numerically solving the Navier–Stokes equation.

Our approach differs in various aspects from previous analyses in the following ways. (i) We do not employ perturbation theory but take into account the full nonlinear interactions of the Navier–Stokes equation. This captures the statistics of the velocity field to any order. (ii) The Reynolds number is rather large, implying an inertial range of two decades. The value of $\zeta(m)$ can be calculated to within 1% up to $m = 8$. We find classical scaling but, surprisingly, no deviations within the error. (iii) Our methods allow to calculate nonuniversal effects on the spectrum, for example, transients or by stirring steady shear profiles. In particular, these latter ones may affect the apparent discrepancy between our finding of classical scaling in "ideal" turbulence and the measured data analysis. (iv) We do not yet take into account spatially varying amplitude statistics ("spatial intermittency"), but temporal intermittency, as provided by chaotically varying mode amplitudes, is properly included. This, in principle, can well lead[23] to corrections of the $\zeta(m)$, the velocity structure function exponents. But, numerically, we found them to be absent within the error.

Details of our ansatz are described in Sec. II. We think that we improve the work by Kerr and Siggia[24] who first studied a decomposition into geometrically scaling wave-number modes, and, also, we actually perform a calculation of the type proposed by Kerr.[25] We choose a consistent interaction between different levels, take other relevant wave numbers, and watch all invariances carefully (for more details of how we differ see Sec. V). Section II also contains the equations of motion, the wave-number hierarchy, and the definition of the *nonstatistical* stirring force.

In Sec. III, we fix the state of high Reynolds number turbulence by choosing the viscosity ν and the rate of dissipation ϵ. A compilation of all relevant quantities of the flow fields considered is documented in Table I.

The structure functions and the spectrum of developed turbulence are discussed in Sec. IV. In particular, we carefully analyze the moment exponents $\zeta(m)$. Within the errors, they do not deviate from the classical scaling $m/3$. The value of the numerical constant b in the structure function (1) is still rather bad, evidently because of the still not-large-enough number of selected modes. Our results for b and $\zeta(m)$ will be summarized in Tables I and II.

In Sec. V, we discuss various relations to previous work, provide more insight into the mechanism of the energy transfer, and extend our analysis to a multilevel fluctuating energy input that models laminar profiles as the origin of turbulence.

II. FOURIER–WEIERSTRASS DECOMPOSITION

The flow field $u_i(\mathbf{x},t)$ is Fourier transformed into plane waves

$$u_i(\mathbf{x},t) = \sum_{\mathbf{p}} u_i(\mathbf{p},t) e^{i\mathbf{p}\cdot\mathbf{x}}. \tag{8}$$

Of course, $u_i^*(\mathbf{p},t) = u_i(-\mathbf{p},t)$ and $\mathbf{p}\cdot\mathbf{u}(\mathbf{p},t) = 0$. A cubic periodicity box of linear extension $2\pi L$ is chosen, so $p_i = \pm n_i/L$, $n_i = 0,1,2,\ldots$. The Navier–Stokes equation for the $u_i(\mathbf{p},t)$ reads

$$\partial_t u_i(\mathbf{p},t) = -iM_{ijk}(\mathbf{p}) \sum_{\mathbf{q}} u_j(\mathbf{q}) u_k(\mathbf{p}-\mathbf{q}) - \nu\mathbf{p}^2 u_i(\mathbf{p}) + f_i(\mathbf{p}). \tag{9}$$

The coupling strength is symmetric in j, k:

$$M_{ijk}(\mathbf{p}) = [p_j P^{\perp}_{ik}(\mathbf{p}) + p_k P^{\perp}_{ij}(\mathbf{p})]/2. \tag{10}$$

Here, $P^{\perp}$ denotes the orthogonal projector and ν is the kinematic viscosity. The external driving force $f_i(\mathbf{p},t)$ will be chosen later; it is *not* assumed to be stochastic, i.e., (9) is a purely deterministic equation.

Since the number of contributing modes in high Reynolds number flow is intractably large, we now restrict the set of allowed wave numbers. The idea is that the presence of an eddy cascade is properly described by a geometrical scaling of the wavelengths, corresponding to

$$(Lp_i)^{-1} = \pm\lambda^{-l_i}, \quad l_i = 0,1,2,\ldots. \tag{11}$$

Our choice of the scaling factor will be $\lambda = 2$. The n_i admitted for the wave numbers p_i are the λ^{l_i} only.

From the allowed wave numbers (11), we select a subset K_l that will form the lth level of our eddy cascade. The next higher level K_{l+1} is obtained by scaling all wave numbers with a *common* factor 2. Thus K_{l+1} corresponds to the next smaller eddies.

It is not possible to work with a single direction in $\mathbf{k}$ space, for example, to restrict the wave numbers to only $\pm L\mathbf{p} = (\lambda^l, \lambda^l, \lambda^l)$, $l = 0,1,2,\ldots$. Each interacting triad $\mathbf{p} = \mathbf{q}_1 + \mathbf{q}_2$ then consists of three vectors in parallel. But because of incompressibility, parallel vectors cannot interact:

$$M_{ijk}(\mathbf{p}) u_j(\alpha_1\mathbf{p}) u_k(\alpha_2\mathbf{p}) = 0.$$

We therefore include other directions in k-space. Our choice is

$$
\begin{aligned}
&2^l(1,\ 1,\ 1),\\
&2^l(-\tfrac{1}{2},\ 1,\ 1), && \text{plus two permutations,}\\
&2^l(1,\ -\tfrac{1}{2},\ -\tfrac{1}{2}), && \text{plus two permutations,}\\
&2^l(\tfrac{1}{2},\ 2,\ 2), && \text{plus two permutations,}\\
&2^l(2,\ \tfrac{1}{2},\ \tfrac{1}{2}), && \text{plus two permutations.}
\end{aligned}
\tag{12}
$$

This mode selection allows for a coupling between different cascade levels, for example, via $(-\frac{1}{2},1,1) + (1,-\frac{1}{2},-\frac{1}{2}) = 2^{-1}(1,1,1)$. Here, the $(-\frac{1}{2},1,1)$—and the $(1,-\frac{1}{2},-\frac{1}{2})$—modes interact with the (1,1,1) mode of the next lower level, i.e., with the larger eddies. There are also many intrashell couplings, e.g., $(-\frac{1}{2},1,1) - (\frac{1}{2},2,2) = -(1,1,1)$. Figure 1 represents the modes of two adjacent levels together with the possible interactions. The directions of the chosen wave vectors are approximately uniform. Equation (12) seems to be the smallest system with these coupling and uniformity properties. Note that, in particular, $p_i = 0$ is not present. Namely, if vanishing vector components would be allowed, this would increase the number of modes by more than a factor of 4, since $(\frac{1}{2},1,1)$, $(\frac{1}{2},-1,1)$, etc., have to be included in addition to $(-\frac{1}{2},1,1)$ for consistency. We therefore define the set K_l as the wave numbers (12) together with the corresponding ones of opposite sign:

$$K_l = \{\pm 2^l(1,1,1), \pm 2^l(-\tfrac{1}{2},1,1),\ldots\}. \tag{13}$$

Here, l runs from the lowest level $l=0$ to the highest level $l=N_\eta$; later, $N_\eta = 10$. So the whole cascade will consist of the wave number set K:

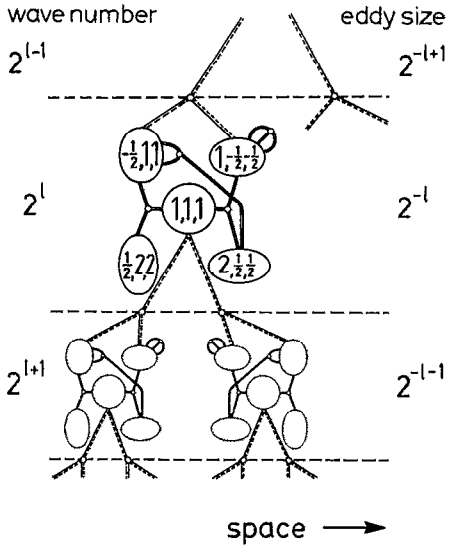

FIG. 1. The hierarchy of interacting wave numbers for the amplitudes $u_i(\mathbf{p},t)$ admitted in the Fourier–Weierstrass plane-wave series for the Eulerian flow field. The classification into levels is such that all $\mathbf{p}$ of one level are transformed by a factor of 2 or 1/2 to the next higher or lower level. The larger the l value, the larger the wave number, the smaller the eddy, the higher (by definition) the level. Compatible with wave-number conservation are either sums or differences of two vectors; if conservation would be violated, we skip that interaction. There are $1 + 4\times 3 = 13$ wave numbers per level.

$$K = \bigcup_{l=0}^{N_\eta} K_l. \tag{14}$$

There are 13 wave numbers per level, 2×13 if the $-\mathbf{p}$ are included. This corresponds to 26 complex mode amplitudes $u_l(\mathbf{p},t)$. Since $u_l^*(\mathbf{p}) = u_l(-\mathbf{p})$, this is equivalent to 26 real amplitudes. There are as many modes for the other two spatial velocity components. Hence, taking care of $\mathbf{p}\cdot\mathbf{u}(\mathbf{p},t) = 0$, we have $2\times 26 = 52$ independent real modes per level l, and altogether on 11 levels $52\times 11 = 572$ real modes for the whole turbulent flow field.

The complete set of amplitudes $\{u_i(\mathbf{p},t) | i = 1,2,3;\ \mathbf{p}\in K\}$ is determined by the coupled set of ordinary differential equations (ODE's) (9), in which equations $\mathbf{p}\in K$, $\mathbf{q}\in K$, and also $\mathbf{p}-\mathbf{q}\in K$ will always be understood from now on. The possible mode interactions are also indicated in Figure 1. They are partly within each level l, and partly they couple two neighboring levels (semibroken lines). Equation (9) together with incompressibility and wave-number restriction to K is our turbulence model, based on the Navier–Stokes equation.

By properly choosing the force $f_i(\mathbf{p})$, we control the input rate T^{in} of the energy. The dissipation rate ϵ must coincide with this, of course. We next control the degree of turbulence by choosing the viscosity ν. The energy contained in one level and the total energy density of the flow field are

$$E_l(t) = \frac{1}{2}\sum_{\mathbf{p}\in K_l} |\mathbf{u}(\mathbf{p},t)|^2, \tag{15a}$$

$$E(t) = \frac{1}{2V}\int_{\text{p.b.}} |\mathbf{u}(\mathbf{x},t)|^2\, d^3x = \sum_{l=0}^{N_\eta} E_l(t). \tag{15b}$$

Here, p.b. denotes the periodicity box with volume $V = (2\pi L)^3$.

In order to check the effect of restricting the admitted wave numbers to K, we introduced a bigger set of wave numbers K_b also. Here, we allow in addition to the wave numbers (12), still another type to belong to each level l:

$$2^l(2,\ -1,\ \tfrac{1}{2}),\quad \text{plus five permutations.} \tag{16}$$

Combining (12) and (16) enlarges the possible interactions considerably. They are visualized in Fig. 2. In particular, there are now three interlevel connections. The corresponding cascade will be called "large cascade" with the wave numbers in K_b. In contrast, the wave-number set of the "small cascade" described before is denoted by K_s.

Since only adjacent levels interact, one obtains an energy balance equation of the form

$$\partial_t E_l(t) = T_{l-1\to l}(t) - T_{l\to l+1}(t) - \nu\sum_{\mathbf{p}\in K_l}\mathbf{p}^2|\mathbf{u}(\mathbf{p},t)|^2. \tag{17}$$

Here, the contribution of the external forces is still omitted. The transfer rates $T_{l\to l+1}$ are defined by

$$T_{l\to l+1} = \frac{i}{2}\sum_{\substack{\mathbf{p}\in K_l\\ \mathbf{q}\in K_{l+1}\\ \mathbf{p}-\mathbf{q}\in K_l\cup K_{l+1}}} M_{ijk}(\mathbf{p})u_i^*(\mathbf{p})u_j(\mathbf{q})u_k(\mathbf{p}-\mathbf{q}). \tag{18}$$

The sum runs over all allowed triads crossing the line between levels l and $(l+1)$. There are precisely one such

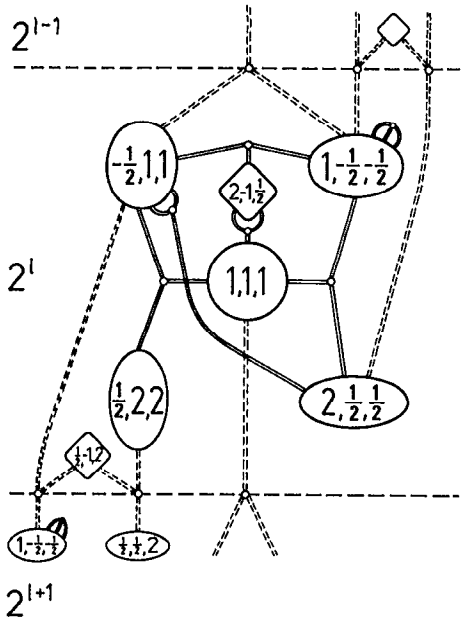

FIG. 2. The large cascade's wave numbers. Instead of only one interlevel interaction, as for the small cascade, there are now three of them. There are $1+4\times3+6=19$ wave numbers per level.

crossing for the small cascade and three for the large cascade. Here, $T_{l\to l+1}$ has the usual meaning of the net energy transfer rate from level l to level $l+1$, i.e., down to smaller eddies.

To produce and maintain a turbulent state as the solution of (9), energy is fed in at a constant rate into some of the largest eddies, i.e., into some modes of the lowest level $l=0$. We model this with a definition of the driving force similar to Kerr and Siggia's[24] for the Burgers model.

$$f_i(\mathbf{p},t)=\frac{\epsilon}{2\cdot6}\sum_{\mathbf{p}_0\in K_{in}}\delta_{\mathbf{p},\mathbf{p}_0}\frac{u_i(\mathbf{p}_0,t)}{|\mathbf{u}(\mathbf{p}_0,t)|^2}. \tag{19}$$

The subset $K_{in}cK_0$ comprises the wave numbers $\pm(-\frac{1}{2},1,1)$, $\pm(1,-\frac{1}{2},-\frac{1}{2})$, and their permutations, i.e.,

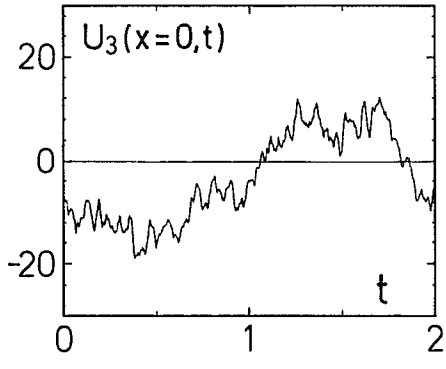

FIG. 3. Shown is the three-component of the velocity field $\mathbf{u}(\mathbf{x},t)$ for a fixed position ($\mathbf{x}=0$) as a function of time t during two turnover times of the largest eddies. The 572 mode amplitudes $u_i(\mathbf{p},t)$ were calculated from the Navier–Stokes equation. The mode superposition is according to (8) but with $\mathbf{p}\in K_{\cdot}$. The Reynolds number is 1.9×10^6, other parameters are documented in Table I. The signal strongly resembles measured velocity signals, see, e.g., Ref. 26.

12 elements. The energy balance equation (17) has to be completed by $\Sigma_{\mathbf{p}\in K_l}u_i^*(\mathbf{p})f_i(\mathbf{p})$. This is $\epsilon\delta_{il_0}$ for the forcing (19).

The numerical solution of Eq. (9) with the driving force (19) shows chaotic behavior on all scales that apparently becomes stationary. Figure 3 displays a typical velocity signal. We shall discuss details later, but will point out that hence we obtained a statistical flow field without any externally applied noise. This verifies the possibility to explain developed turbulence as the stochastics generated by deterministic nonlinear equations, at least in this hierarchical wave-number truncated model. The statistical properties are uniquely determined by the Navier–Stokes equation (viz., its numerical solution). All questions of interest can be explicitly answered, such as, e.g., correlation functions, structure functions, intermittency, etc.

Averages performed according to the deterministic chaos statistics are defined as time averages over the mode amplitudes $u_i(\mathbf{p},t)$ and products thereof of any order. They will be denoted by single brackets $\langle\cdots\rangle$. Because of the restriction of the wave vectors to K, the flow field (8) needs not be exactly statistically translational and rotational invariant. We checked dynamical averages like $\langle u_i(\mathbf{p},t)\rangle$, $\langle u_i^*(\mathbf{p}_1,t)u_j(\mathbf{p}_2,t)\rangle$, and found them to be negligibly small. [To be precise, the former were less than 2% of $\sqrt{\langle u_i^2(\mathbf{p},t)\rangle}$, the latter $\lesssim2\%$ of $\sqrt{\langle u_i^2\rangle\langle u_j^2\rangle}$, $i\neq j$, $\mathbf{p}_1\neq\mathbf{p}_2$.] In order to formally guarantee homogeneity and isotropy, we $\mathbf{y}$-averaged $e^{i\mathbf{p}\cdot(\mathbf{x}+\mathbf{y})}$ in all moments and angle-averaged all $\mathbf{x}$ directions; this averaging is denoted by an additional bracket. Altogether $\langle\langle\cdots\rangle\rangle$ is the ensemble and translation/rotation mean.

Two remarks might be useful. We also coupled the stirring force to only one $\mathbf{p}\in K_0$, mimicking anisotropy; nevertheless the chaotic solutions of (9) with wave numbers restricted to K restored statistical homogeneity and isotropy on the levels $l>0$. The set K is constructed symmetrically with respect to the $i=1,2,3$ axes, but not with respect to continuous rotation; therefore the angle average is *necessary* to ensure isotropy.

An average of particular interest is the structure function

$$D(r)=\langle\langle|\mathbf{u}(\mathbf{x}+\mathbf{r})-\mathbf{u}(\mathbf{x})|^2\rangle\rangle$$
$$=2\sum_{\mathbf{p}\in K}\langle|\mathbf{u}(\mathbf{p})|^2\rangle\left(1-\frac{\sin(rp)}{rp}\right). \tag{20}$$

The dynamical information is contained in the $|\mathbf{u}(\mathbf{p},t)|^2$ average. The longitudinal structure functions are

$$D_{\parallel}^{(m)}(r)=\langle\langle\{[u_i(\mathbf{x}+\mathbf{r})-u_i(\mathbf{x})]r_i/r\}^m\rangle\rangle. \tag{21}$$

Here, $D_{\parallel}^{(1)}=0$ by homogeneity, $D_{\parallel}^{(2)}(r)$ represents the same information as $D(r)$ by incompressibility, as $D=3D_{\parallel}^{(2)}+r\,\partial_r D_{\parallel}^{(2)}$, and $D_{\parallel}^{(3)}$ is related to $D_{\parallel}^{(2)}$ by the Kolmogorov structure equation

$$D_{\parallel}^{(3)}(r)=6\nu\,\partial_r D_{\parallel}(r)-4\epsilon r/5. \tag{22}$$

This is a consequence of the Navier–Stokes equation (9) if only $rp\ll1$ for all modes that receive external energy input. This is the case if there is energy input at the largest eddies only[1,27] (see also, the Appendix). Equation (22) remains

valid for our K-restricted model. It implies $\zeta(3) = 1$ for the inertial range, as usual.

It is straightforward to verify that the average of (4) is identical to the parameter ϵ in the force (19),

$$\langle\langle \epsilon(\mathbf{x},t)\rangle\rangle = \langle\langle \mathbf{u}(\mathbf{x},t)\cdot\mathbf{f}(\mathbf{x},t)\rangle\rangle = \epsilon, \tag{23}$$

i.e., the energy input rate equals the energy dissipation rate.

A serious flaw of the hierarchical cascade model with plane waves introduced here is that certain spatial fluctuations are not admitted. Consider, for example, a large eddy on level $l = 0$. Its contribution to $\mathbf{u}(\mathbf{x},t)$ in (8) is coherent in the entire box $(2\pi L)^3$, fine. It interacts with several half-sized eddies of level $l = 1$. We describe these with amplitudes u_i $(\mathbf{p},t)$ of plane waves $\exp(i\mathbf{p}\cdot\mathbf{x})$, $\mathbf{p}\in K_1$, and $\mathbf{x}\in$box L^3. So they also contribute coherently in the *entire* box. Our cascade model presently still neglects that smaller eddies at different positions in the box should be represented by independent amplitudes u_i $(\mathbf{p};\mathbf{x},t)$. In Fig. 1, the two eddy subsets of level $l+1$, for instance, deserve *independent* mode amplitudes, but we took the same.

We have studied the effect of independent branching in Ref. 23. It contributes essentially to spatial intermittency, visible, e.g., in the ϵ correlation. But it does not influence appreciably the structure functions, which are dominated by eddies of size $\geqslant r$, which, in fact, *are* coherent on the scale r. Since we restrict ourselves to coherent branching, we cannot study all of the intermittency effects mentioned in the Introduction. We concentrate on the structure function exponents $\zeta(m)$.

There is a simple physical reason why the $\epsilon(\mathbf{x},t)$ fluctuations are relatively independent of the exponent deviations $\delta\zeta(m)$ of the structure function if turbulence is modeled by a hierarchical Fourier–Weierstrass decomposition. This is because $\epsilon(\mathbf{x},t)$ is highly dominated by the highest level (smallest eddies) amplitudes, $l = N_\eta$, while in the $D(r)$ sum (20), the terms $l \cong r^{-1}$ dominate. We have studied this quantitatively and in detail.[23] However, since independent spatial branching is not admitted, we can study with some confidence only the effect of temporal statistics ("temporal intermittency") on $\zeta(m)$. Spatial intermittency deserves further study.

III. THE STATE OF DEVELOPED TURBULENCE

We now study the numerical solutions of the system of differential equations (9) with K restriction as described above. All lengths are henceforth measured in units of L; so the periodicity length is 2π. The time unit T is chosen to make the dissipation rate ϵ in units L^2T^{-3} equal to 1; i.e., we have $T = L^{2/3}\epsilon^{-1/3}$. The velocities u_i $(\mathbf{x})$ and u_i $(\mathbf{p})$ are measured in $L/T = (L\epsilon)^{1/3}$. Here, ν comes in multiples of L^2T^{-1}, i.e., of $L^{4/3}\epsilon^{1/3}$. In the nondimensionalized Navier–Stokes equation, ν^{-1} then is the natural Reynolds number $\mathrm{Re} = L^2T^{-1}/\nu$. The force f_i $(\mathbf{x},t)$ is measured in LT^{-2} or $L^{-1/3}\epsilon^{2/3}$. We keep $L,x,t,u,\nu,\epsilon,\ldots$, for the dimensionless quantities.

The time unit can be interpreted as the Kolmogorov time of the largest eddies, the velocity unit as their Kolmogorov velocity.

In our simulations, we took 11 levels $l = 0$ to $l = N_\eta = 10$. The kinematic viscosity ν was adjusted such that the energy in an additional 12th level came out to be practically zero. Hence this level could safely be omitted. Typical values of ν are 0.5 to 2 times 10^{-6}, e.g., $\mathrm{Re} \approx 10^6$.

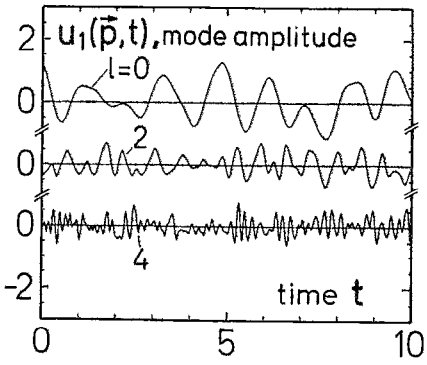

FIG. 4. The time dependence of the 1-component of the modes u_i $(\mathbf{p},t)$, $L\mathbf{p} = 2^l(1,1,1)$, of level $l = 0$ (largest eddy), 2, and 4. The time is measured in units of the largest eddy's turnover time $T = L^{2/3}\epsilon^{-1/3}$, the amplitudes u_i in units of $L/T = (L\epsilon)^{1/3}$. The typical $l = 0$ velocity is ≈ 0.86, the mean values $\langle u_i\rangle$ are about 10^{-2}. The parameters are those of the small cascade (572 modes), see Table I. A transient period of 50 or more is skipped.

Figure 4 shows the stationary oscillations of the (1,1,1) modes of levels 0, 2, and 4 around their mean value 0. The same typical behavior is shown by the other modes, too. Apparently the amplitudes u_i $(\mathbf{p},t)$ and thus the velocity field (8) are chaotic. To check the chaotic time dependence of the solutions, we consider the time correlation function of one mode amplitude, see Fig. 5. For time separations greater than 3, there is complete decorrelation.

The three modes shown in Fig. 4 seem to behave in time qualitatively alike. This can be made even more convincing, if the time scale and the amplitude scale are properly adjusted. According to the classical scaling theory of turbulence,[3-7] one expects

$$\text{amplitude} \propto \lambda^{-l/3}, \quad \text{time} \propto \lambda^{-2l/3}. \tag{24}$$

To check the validity of (24), we consider the energy E_l contained in the l th level, see Fig. 6. The classical scaling law

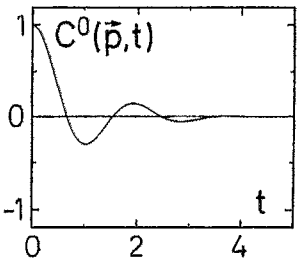

FIG. 5. The real part C^0 $(\mathbf{p},t)$ of the normalized autocorrelation function $\langle \mathbf{u}^*(\mathbf{p},0)\cdot\mathbf{u}(\mathbf{p},t)\rangle/\langle|\mathbf{u}(\mathbf{p})|^2\rangle$ of the eddy $L\mathbf{p} = (1,1,1)$ of level $l = 0$ as it decays with time t. The time decorrelation of other modes is similar but on time scales $\propto 2^{-2l/3}$. Time is measured in the largest eddy's turnover time $T = L^{2/3}\epsilon^{-1/3}$. Note the oscillatory decay, which seems to indicate that the lowest-order continued fraction calculation for the Lagrangian decay rates[27] is not quite sufficient. The parameters of the small cascade (572 modes) are used, cf. Table I.

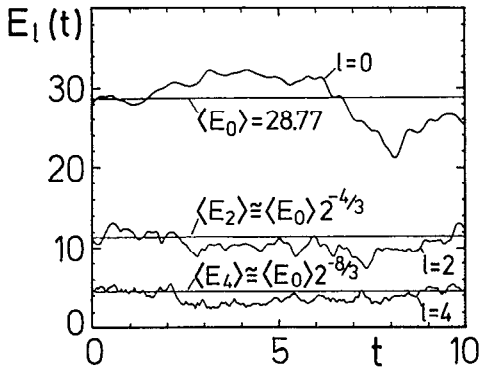

FIG. 6. The time behavior of $E_l(t)$, $l=0,2,4$, shows small-scale fluctuations whose typical time and magnitude seems to decrease $\propto 2^{-2l/3}$. In addition, one observes larger and longer lasting meandering, therefore we averaged all relevant means at least over periods of 100 and even much longer (up to 1000 turnover times). Time is measured as usual in multiples of the largest eddy's turnover time $L^{2/3}\epsilon^{-1/3}$. The mean energies (straight lines) scale pretty accurately as $2^{-2l/3}$. Numerically, for the parameters of the small cascade (cf. Table I), $\langle E_0\rangle = 28.77$. (For the large cascade, we found $\langle E_0\rangle = 32.37$, and for the multilevel input, see Sec. V, $\langle E_0\rangle = 13.71$.)

is obviously confirmed. This is not *a priori* trivial but reflects a property of the numerical solution of our Fourier–Weierstrass analysis of turbulence. We can understand it qualitatively from the energy balance equation (17). In the inertial range of scales, where ν can be neglected, and there is no input, we obtain for stationary states

$$\langle T_{l\to l+1}\rangle = \epsilon. \tag{25}$$

Since $T_{l\to l+1}$ is of third order in the amplitudes, the u amplitudes are expected to scale approximately like $2^{-l/3}$ and E_l as $2^{-2l/3}$. However, one should remember the possibility of a buildup of fluctuations while the energy cascades down.[24] It is not at all trivial that these fluctuations are self-similar nor that they are small. In fact, one does not even come close to the classical scaling (24), if the Burgers equation is considered and treated analogously;[24] cf. Sec. V. Figure 7 shows

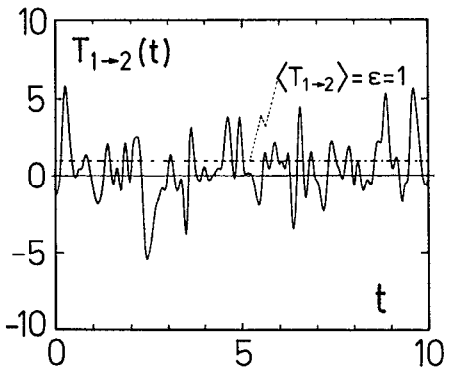

FIG. 7. The large fluctuations of the rate of energy transfer $T_{1\to 2}(t)$ from level $l=1$ to level $l=2$ as a function of time. The mean value $\langle T_{1\to 2}\rangle$ (dashed line) agrees very well with the energy input rate ϵ, i.e., 1. The numerical integration was performed with the parameters of the small cascade. The typical time in $T_{1\to 2}$ is comparable with that of level 2.

the actual temporal behavior of the transfer rates $T_{l\to l+1}(t)$ in the present approach.

We now report the various characteristic numbers of the turbulent state that we realize numerically. For the small cascade we take $\nu = 5.4\times 10^{-7}$ and, as stated, $\epsilon = 1$, $L = 1$. The Kolmogorov length and velocity are $\eta = (\nu^3/\epsilon)^{1/4} = 2.0\times 10^{-5}$ and $v_\eta = (\nu\epsilon)^{1/4} = 2.7\times 10^{-2}$. Then the Re number is $\mathrm{Re} = \nu^{-1} = 1.9\times 10^6$ and $\mathrm{Re} = (L/\eta)^{4/3}$ without any additional factor. The Taylor microscale is defined by $\lambda_T = \sqrt{\langle\langle u_1^2\rangle\rangle/\langle\langle(\partial_1 u_1)^2\rangle\rangle}$. The value of $\langle\langle(\partial_1 u_1)^2\rangle\rangle$ can be calculated via the well-known relation $\langle\langle(\partial_1 u_1)^2\rangle\rangle = \epsilon/15\nu$ and $\langle\langle u_1^2\rangle\rangle$ is given by $(1/3)\Sigma_{\mathbf{p}\in K}\langle|\mathbf{u}(\mathbf{p})|^2\rangle$, or $(2/3)\Sigma_l\langle E_l\rangle$. Assuming that the mode energies $\langle|\mathbf{u}(\mathbf{p})|^2\rangle/2$ scale, to a good accuracy, as $2^{-2l/3}$ this gives (extrapolating the ISR to infinity)

$$\langle\langle u_1^2(x)\rangle\rangle = \frac{1}{3(1-2^{-2/3})}\sum_{\mathbf{p}\in K_0}\langle|\mathbf{u}(\mathbf{p})|^2\rangle = 1.80\langle E_0\rangle.$$

The largest level's sum $\langle E_0\rangle$ was evaluated numerically to give $\langle\langle u_1^2\rangle\rangle = 52$, so that $\lambda_T = 0.021$. This finally gives the Taylor–Reynolds number $\mathrm{Re}_\lambda = \sqrt{\langle\langle u_1^2\rangle\rangle}\lambda_T/\nu = 2.73\times 10^5$. Table I contains all these characteristic parameters and physical quantities of the small cascade together with the corresponding values for the large cascade and the multilevel input cascade, which will be explained in Sec. V.

Note that our model allows a fairly well developed turbulence. The Taylor–Reynolds number $\mathrm{Re}_\lambda \approx 273\,000$ should be compared with $\mathrm{Re}_\lambda \approx 4300$ in typical atmospherical measurements (estimated in Ref. 27 using data of Ref. 28). One might wonder about the relation between Re and Re_λ. There still holds the relation

$$\mathrm{Re}_\lambda = \varkappa\,\mathrm{Re}^{1/2} = \varkappa(L/\eta)^{2/3}. \tag{26}$$

But the value of $\varkappa$ is characteristic for the dynamics of the cascade, and therefore related to b. In Ref. 23 we derive for a one-dimensional Fourier–Weierstrass model

$$\varkappa = 0.50b. \tag{27}$$

Using the experimental value $b = 8.4$, one recovers the value $\varkappa = 4.24$ known from the literature[28] and implying $\mathrm{Re}_\lambda \approx \sqrt{\mathrm{Re}}$. For the small cascade here, however, $b = 300$, so $\varkappa = 150$; the large cascade has $\varkappa = 86$. With these $\varkappa$'s, Eq. (26) is in agreement with the numbers quoted in Table I.

If $\mathrm{Re} = \nu^{-1} = 1.9\times 10^6$ is used together with the realistic value of $\varkappa = 4.24$ in (26), our turbulence still has the unusually large Taylor–Reynolds number $\mathrm{Re}_\lambda \approx 6000$.

IV. STRUCTURE FUNCTION AND SPECTRUM

We begin with a discussion of the second-order structure function $D(r)$. To produce Fig. 8, we directly used (20) with the moments $\langle|\mathbf{u}(\mathbf{p})|^2\rangle$ calculated numerically for the small cascade. For comparison, Batchelor's[29] interpolation for $D(r)$ is also shown,

$$D_{\mathrm{Batch}}(r) = \frac{1}{3}v_\eta^2\left(\frac{r}{\eta}\right)^2\left[1+(3b)^{-3/2}\left(\frac{r}{\eta}\right)^2\right]^{-2/3}, \tag{28}$$

which coincides with (1) if $r\in$ISR. The only free parameter in (28) is the numerical factor b. We can determine it by

TABLE I. The physical parameters of the various eddy cascades. The first row contains the number of real modes and of levels; 11 levels correspond to 3 decades. All physical quantities are dimensionless, lengths being measured in multiples of L, dissipation rates in those of ϵ, times of $L^{2/3}\epsilon^{-1/3}$, velocities of L/T or $(L\epsilon)^{-1/3}$. The periodicity box is 2π, length 1, dissipation rate 1 or 0.35, respectively. The energy input rates are constant and on the largest eddy level $l=0$ only (first two columns) or they fluctuate and contribute on several levels resulting from basic laminar parabolic profile. The kinematic viscosity is ν, its inverse the bare Reynolds number. The Kolmogorov internal (viscous) length scale is $\eta=(\nu^3/\epsilon)^{1/4}$ and the corresponding velocity $v_\eta=(\nu\epsilon)^{1/4}$. The mean turbulent shear is $\sqrt{\langle\langle(\partial_1 u_1/\partial x_1)^2\rangle\rangle}=\sqrt{\epsilon/(15\nu)}$. All these quantities are externally controlled parameters if ν, ϵ are given. The other quantities contain dynamical information about the cascade and were obtained numerically. The quantity U_L is a measure of the typical mode amplitude for any of the largest eddies, $U_L^2/2=\langle E_0\rangle/[3\cdot 2\cdot(13 \text{ or } 19)]$; U_L can be read from Fig. 4, for example, with $\langle E_0\rangle$ in Fig. 6. The rms of the velocity [see Eq. (8)] fluctuations in position space is $\sqrt{\langle\langle u_1^2(x)\rangle\rangle}$. The value b denotes the prefactor in the inertial range structure function (1), determined in Sec. IV; in the multilevel input flow, we do not determine a value b since in parts of the inertial range, there still is $\langle T_l^{in}\rangle\neq 0$. The Taylor length λ_T and the Taylor–Reynolds number Re_λ are defined as usual. Note the impressive degree of turbulence, quantified by $\mathrm{Re}_\lambda\approx 273\,000$ or, with the physical b using (26) and (27), $\mathrm{Re}_\lambda\approx 6000$. The last line contains the numerical values of $\langle E_0\rangle$, the largest eddy level energy, on which various other physical quantities are based.

Physical quantity	Small cascade 52 modes per level, 11 levels	Large cascade 76 modes per level, 11 levels	Small cascade parabolic profile multilevel input
Number of real modes	572	836	572
Energy input rate	only $l=0, T_0^{in}=1$	only $l=0, T_0^{in}=1$	$\langle T_0^{in}\rangle=0.30$
Dissipation rate ϵ	1	1	0.35
Viscosity ν	0.54×10^{-6}	2.4×10^{-6}	0.40×10^{-6}
Viscous length η	2.0×10^{-5}	6.1×10^{-5}	2.1×10^{-5}
Viscous velocity v_η	0.027	0.039	0.019
$\mathrm{Re}=\nu^{-1}$	1.9×10^{6}	4.2×10^{5}	2.5×10^{6}
U_L	0.86	0.75	0.59
$\sqrt{\langle\langle u_1^2(x)\rangle\rangle}$	7.2	5.4	5.0
b	300	171	...
$\sqrt{\langle\langle(\partial u_1/\partial x_1)^2\rangle\rangle}$	351	167	242
λ_T	0.021	0.032	0.021
Re_λ	273 000	73 000	255 000
$\langle E_0\rangle$	28.77	32.37	13.71

evaluating the exact expression (20) for $D(r)$. As we already pointed out, the energies $\langle|\mathbf{u}(\mathbf{p})|^2\rangle$ scale with $\mathbf{p}$ in sufficient accuracy as $2^{-2l/3}$; this will be checked and confirmed once more later in this section. We then apply Poisson's sum formula for $r\in$ISR and get

$$D(r)=2\frac{3\Gamma(-2/3)\sin(-\pi/6)}{5\ln 2}\times\left(\sum_{\mathbf{p}\in K_0}|\mathbf{p}|^{2/3}\langle|\mathbf{u}(\mathbf{p})|^2\rangle\right)r^{2/3}. \tag{29}$$

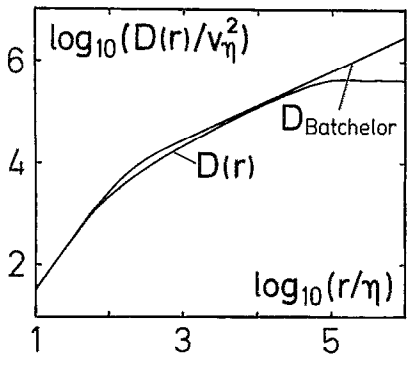

FIG. 8. Scale dependence of the structure function (delta variance) $D(r)$. The inertial subrange (ISR) comprises about 2 decades. Near the transition to the viscous subrange (VSR) the viscosity lowers the numerical, Navier–Stokes-based curve stronger than Batchelor's interpolation formula says. If we decrease ν, i.e., increase Re further, both curves tend to agree even more.

The remaining sum over $\mathbf{p}\in K_0$ was calculated numerically giving the value 86.2. Comparing now (29) with (28) in the ISR leads to the value of b in our turbulent Navier–Stokes flow. We find for the small cascade (cf. Table I) $b=300$.

This value is considerably larger than the experimental value of 8.4. We think this can be understood by phase space considerations.[30] If one adds more modes to the small cas-

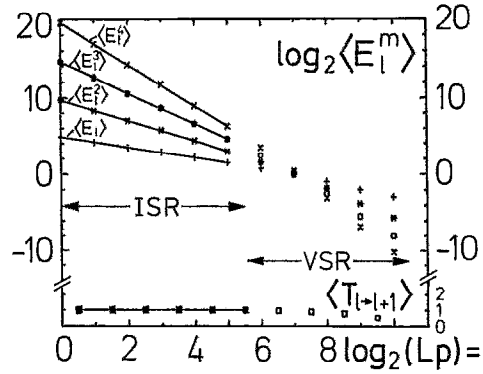

FIG. 9. Spectrum $\langle E_l\rangle$ versus eddy level l, i.e., versus wave number p, together with some moments. The ordinate shows $\log_2$ of the moments $\langle E_l^m\rangle$. In the bottom part, the mean transfer rates between adjacent levels are plotted on a separate scale; in the inertial range they are 1, of course. All lines are rms fits. After omitting a transient of 50 turnover times, the averaging time is 1200. For the physical parameters of the small cascade, cf. Table I. The scaling $\langle E_l^m\rangle\propto p^{\zeta(2m)}$ with $\zeta(2m)=2m/3$ is quite accurate. The decrease of $\langle E_l^m\rangle$ in the viscous subrange is less than expected.

TABLE II. Computed values of moment scaling exponents $\zeta(m)$ and comparison with the corresponding numbers from the analysis of experiments by Anselmet *et al.*[8] We estimated the statistical errors with the common χ^2 routine.[31] The averaging times t_{av} for $\langle E_l^m \rangle$ for the small cascade was 1200, although an increase from 400 to 1200 influenced $\delta\zeta(m)$ by less than the statistical error. In the multilevel case, we used $t_{av} = 2000$, for the big cascade 200.

Moment exponent deviation	$\langle E(p) \rangle \propto p^{-\zeta(2)}$ $\delta\zeta(2) = \zeta(2) - 2/3$	$\langle E^2(p) \rangle \propto p^{-\zeta(4)}$ $\delta\zeta(4) = \zeta(4) - 4/3$	$\langle E^3(p) \rangle \propto p^{-\zeta(6)}$ $\delta\zeta(6) = \zeta(6) - 6/3$	$\langle E^4(p) \rangle \propto p^{-\zeta(8)}$ $\delta\zeta(8) = \zeta(8) - 8/3$
Experiment	0.04	0.00	− 0.20	− 0.45
Small cascade $T_0^m = 1$	0.012 ± 0.002	0.013 ± 0.006	0.001 ± 0.013	− 0.022 ± 0.020
Large cascade $T_0^m = 1$	0.014 ± 0.003	0.015 ± 0.008	0.003 ± 0.015	− 0.023 ± 0.030
Small cascade quadratic profile four-level ISR	− 0.008 ± 0.015	− 0.027 ± 0.027	− 0.057 ± 0.036	− 0.098 ± 0.047
Small cascade quadratic profile six-level ISR	0.006 ± 0.007	0.003 ± 0.014	− 0.006 ± 0.021	− 0.021 ± 0.030
Small cascade linear profile four-level ISR	− 0.093 ± 0.033	− 0.190 ± 0.068	− 0.292 ± 0.104	− 0.399 ± 0.141
Small cascade linear profile six-level ISR	− 0.040 ± 0.021	− 0.087 ± 0.042	− 0.142 ± 0.063	− 0.203 ± 0.084

cade, the number of permitted interlevel wave-vector triads grows quadratically with the number of modes. So the energy transport becomes more effective, lowering the value of b. In fact, we have also calculated b for the large cascade, which gave the smaller value $b_b = 171$.

Let us consider now the spectrum of the flow field. Figure 9 shows the moments $\langle E_l^m \rangle$ for $m = 1,2,3$, and 4. The length of the inertial range was defined so that the data could faithfully be fitted by straight lines with sufficiently small scatter. In the inertial range, relation (25) is fulfilled to within 0.5%.

The slopes were obtained by a least square fit to the data in the ISR, the results are listed in Table II together with the corresponding variances of the $\zeta(m)$. For comparison, we also give the $\zeta(m)$ values of the experiments of Anselmet *et al.*[8]

In general, the scaling exponents lie near $m/3$ within the variances. So we find no significant corrections to the classical scaling values. Of course, there remain systematic errors due to the finite width of the ISR. So we think that the high values for $\zeta(2)$ and $\zeta(4)$ show the influence of viscosity, since $\delta\zeta(2)$ and $\delta\zeta(4)$ should have opposite sign, if the corrections were induced by intermittency.

We repeated the procedure for shorter averaging times and found the χ^2 value of the fit to go down in time. Thus the data fit a straight line sufficiently well only in a long time limit of considerable length that might not always be guaranteed in the analysis of experiments.

To check a possible influence of the number of modes on the values of the exponents $\zeta(m)$, we repeated the analysis for the large cascade. We still did not find significant corrections to classical scaling, see Table II. In fact, convergence of the moments was faster than for the small cascade, so the fluctuations seem to *decrease* by adding more modes.

It would be interesting to proceed further and include vector components with $Lp_i \in \pm 2^l\{2,3\}$ or $Lp_i \in \pm 2^l\{4,5,6\}$ and so forth. This allows for interactions between more distant levels. The influence of nonlocal energy transfer could thus be studied systematically.

V. DISCUSSION

Similar to our ansatz, Kerr and Siggia[24] analyzed the Burgers equation with the one-dimensional decomposition of the flow field

$$u(x,t) = \sum_{p \in K} u(p,t) e^{ipx}, \quad K = \{ \pm \lambda^l, 0 \leqslant l \leqslant N_\eta \}. \quad (30)$$

Each cascade level is represented by one complex mode. The energy balance equation (17) stays intact, but the system looses its complicated intrashell dynamics, which seems to be responsible for the typical time dependence of the amplitudes shown in Fig. 4. In our cascade, we found that the mode set consisting of the wave numbers of a single level gives qualitatively the same chaotic solutions. In the Burgers system, by contrast, this is not so. For the whole coupled set of mode equations, two different types of "collective" behavior can be observed. As reported by Lee,[32] if the energy is removed consistently by viscosity, the solutions approach a steady state that is globally stable. The system shows no stochastic behavior and has lost its time scale.

Kerr and Siggia[24] substituted the viscous terms by phenomenological eddy damping terms of second order in the velocity. Then the stationary solution becomes unstable and the energy is transported in "bursts" traveling through the cascade. To this type of collective behavior the arguments of Sec. III, giving the approximate scaling form of $u_i(\mathbf{p},t)$, do not apply. So the authors[24] were not able to infer scaling exponents from their simulations, though working with up to 12 levels. In our mode system, we did not find evidence for traveling pulses from plotting the time dependence of the various energy transfer rates, but we cannot exclude that more sophisticated techniques (as introduced by Kerr[33]) might reveal pulselike behavior. Kerr found indications for pulse formation in his simulations of Navier–Stokes flow.

An earlier work of Siggia[24] is based on the 3-D Navier–Stokes equation. He chooses a set of wave numbers different from ours, namely,

$$K_l = \{2^l(e_1,e_2,e_3),\ e_i = \pm 1,0;(e_1,e_2,e_3)\neq 0\}. \quad (31)$$

But instead of coupling the modes by the Navier–Stokes interaction, a modified set of equations was introduced, where momentum conservation $\mathbf{p} = \mathbf{q}_1 + \mathbf{q}_2$ between the wave vectors of an interacting triad is satisfied only approximately. This leads to equations, where any mode of one level is coupled to all modes of the two adjacent levels. The resulting time dependence of the energy E_l (t) or the energy transfer rate $T_{l\to l+1}$ (t) is dramatically different from the results shown in Figs. 6 and 7.

To analyze the difference between Ref. 24 and our solution in more detail, we simulated a 4-level system with different interaction structure. The interlevel energy *loss* via the symmetric mode $2^l(1,1,1)$ is skipped. Instead, *each* mode of a given level l gets a loss term by adding (like in Ref. 24, second approximation)

$$-(T_{l\to l+1}/2E_l)u_i(\mathbf{p},t) \quad (32)$$

in Eq. (9). The interlevel energy input is kept. This new system conserves energy [as described by (17)] and momentum but violates Galilean invariance, since E_l and $T_{l\to l+1}$ are not Galilean invariant quantities. As in the case of Siggia's model, we found that its solutions show no resemblance to the previous results anymore. In particular, the characteristic classical time scale $\propto \epsilon^{-1/3} r^{2/3}$ is completely lost. So we conclude that it is important for the success of our method that the truncated equations still share the invariances of the original Navier–Stokes equation.

The case of Galilean invariance still deserves some comments. Since K does not contain the null vector, Galilean invariance is formally violated. However, two neighboring levels couple in a Galilean invariant manner, and convection effects of more distant levels are not present, since they were skipped by ansatz. A similar mechanism was analyzed in Ref. 30.

Even if they still miss the complete Navier–Stokes equation, our restricted equations (9) with K_s or K_h should be of interest in their own right, because they allow to study nonperturbatively any aspect of turbulent phenomena by direct simulation.

We now address the question of possible corrections to the classical scaling. Can one understand the experimental findings, which show (though somewhat inconclusively) intermittency corrections within our plane-wave analysis. We consider two different possible mechanisms to account for these corrections

(1) The external force need not be of the form (19). In fact, in real flows, pressure differences or external shear induce a basic laminar steady profile $U_i(\mathbf{x})$, which is a stationary solution of the Navier–Stokes equation. If we write the total velocity field as the sum of $U_i(\mathbf{x})$ and a fluctuating field $u_i(\mathbf{x},t)$ we obtain for this $u_i(\mathbf{x},t)$ an equation of motion (9) with a force, which is linear in both U_i and u_i,

$$f_i(\mathbf{p},t) = -2iM_{ijk}(\mathbf{p})\sum_{\mathbf{q}} u_j(\mathbf{q})U_k(\mathbf{p}-\mathbf{q}). \quad (33)$$

The Fourier amplitudes $U_k(\mathbf{p})$ of the laminar profile $U_k(\mathbf{x})$ provide a force (33) that acts on *all* scales and not only on the $l=0$ level. There is a mean energy input $\langle T_l^{\text{in}}\rangle = \Sigma_{\mathbf{p}\in K_l}\langle u_i^*(\mathbf{p})f_i(\mathbf{p})\rangle$ into all levels l. If the Fourier components of U scale like $|\mathbf{q}|^{-\alpha}$, one expects an estimate

$$\langle T_l^{\text{in}}\rangle \propto \langle E_l\rangle 2^{(1-\alpha)l} \approx \langle E_0\rangle 2^{(1/3-\alpha)l}.$$

The laminar profile of the plane Poiseuille problem, for example, is given by

$$U_k(\mathbf{x}) = Ux_3(1-x_3)\delta_{1k}, \quad 0\leqslant x_3\leqslant 1. \quad (34)$$

This gives $\alpha = 2$, so the energy input is still dominated by $\langle T_0^{\text{in}}\rangle$, and the exponents of sufficiently high levels are unchanged. However, over a limited range of scales $0\leqslant l\leqslant l_{\text{in}}$, the total input $\langle T_l^{\text{in,tot}}\rangle = \Sigma_{l'=0}^{l}\langle T_{l'}^{\text{in}}\rangle$ still increases with l leading to less decrease of the $\langle E_l\rangle$. If the modified spectra are nevertheless fitted by a pure power law, this will have a corrected exponent. As an example, we simulated the small cascade with a force that mimics the essential features of (33) with the parabolic profile (34),

$$f_i(\mathbf{p}) = 2iUP_{i1}^{\perp}(\mathbf{p})\sum_l 2^{-l}u_2(\mathbf{q}(\mathbf{p},l)). \quad (35)$$

Here, $\mathbf{q} = \mathbf{q}(\mathbf{p},l) = (p_1,p_2,\lambda^l - p_3)$ shall be $\in K$; the possible case $\mathbf{q} = \mathbf{p}$ is omitted, since it would correspond to a contribution of $U_k(\mathbf{p}-\mathbf{q}=0)$ in (33), although a mean velocity does not feed in energy. If the driving laminar profile is linear instead of quadratic, as in (34), one only has to skip the factor 2^{-l} in (35).

Figure 10 shows the strongly fluctuating energy input rate into the lowest level. The input parameter ϵ no longer appears in our equations. Nevertheless, a finite value of $\langle T_0^{\text{in}}\rangle$ adjusts itself for a given value of U. For $U=0.4$, we obtained $\langle T_0^{\text{in}}\rangle = 0.30$ after the cascade became stationary. The transfer rates between the lowest levels increase slightly, because there is also input for $l>0$. The numerical values for the input rates are $\langle T_l^{\text{in}}\rangle = 0.303,\ 0.039,\ 0.004,\ 0.0004...$, $l = 0,1,2,3,...$, which agrees roughly with our previous estimate.

We determined the exponents $\zeta(m)$ by fitting a straight line in two slightly different manners. We chose first (cf. Fig. 11) a reduced inertial range, which comprises only the first four levels, as one often has in real experiments. The resulting values of $\zeta(m)$ may be found in Table II. The deviations $\delta\zeta(m)$ are not large enough to fully account for the experi-

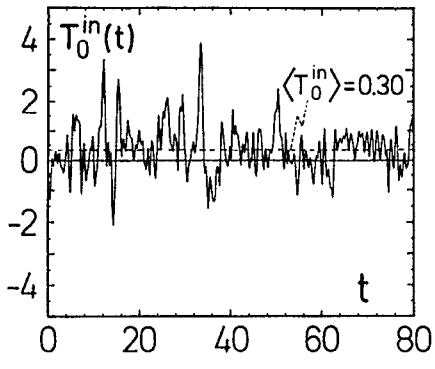

FIG. 10. The rate of energy input into the lowest level $l = 0$ (largest eddies) as provided by the parabolic driving laminar profile, cf. (34) and (35). Since $f \propto u$, we have $T_0^{in} \propto uu$, so $T_0^{in}(t)$ reflects the strong fluctuations of the solution $u_l(\mathbf{p}, t)$. There is momentary input as well as output but the average input rate is positive (dashed line at 0.30). The turnover time of the largest eddy here is $L^{2/3}\langle T_0^{in}\rangle^{-1/3} = 0.30^{-1/3} = 1.49$; this is visible as a typical time scale (abscissa in the usual units, cf. Sec. III).

mental findings, but they are significantly larger than for constant ϵ input. Second, we extended the inertial range to six levels, as we had before. This time the same numerical data yield smaller corrections $\delta\zeta(m)$, see Table II.

For a linear shear profile it is $U_l(q) \propto q^{-1}$ (i.e., $\alpha = 1$), so 2^{-l} in the force (35) has to be skipped. The input rates $\langle T_l^{in}\rangle$ decrease slower with l and the total input up to level l grows even more pronounced. The exponent corrections are visible in Fig. 11. The slope evidently depends appreciably on the chosen length of the ISR. The increase of $\langle E_l^m\rangle$ with l can approximately be explained with the initial increase of $\langle T_l^{in,tot}\rangle$, since $\langle E_l^m\rangle \propto \langle T_l^{in,tot}\rangle^{2m/3}$.

(2) Another possible reason for deviations of $\zeta(m)$ from $m/3$ might be that the cascade has not yet reached a stationary state.

If the energy distribution initially deviates significantly

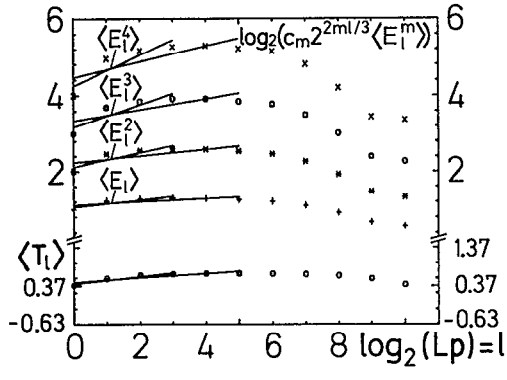

FIG. 11. Spectrum $\langle E_l\rangle$ and some moments $\langle E_l^m\rangle$ for $m = 2,3,4$ as functions of the wave number $p \propto 2^l$. The classical scaling $2^{-2ml/3}$ has been subtracted, i.e., any nonclassical exponent correction is visible as a deviation from a horizontal line. The value c_m is chosen such that the $m = 1$ curve starts at 1, the $m = 2$ moment from 2, etc. The small cascade is simulated; the driving laminar profile is linear; the averaging time (after transients) is 900. The deviations $\delta\zeta(m)$ are reported in Table II. Bottom curve $\langle T_l\rangle = \langle T_l^{in}\rangle + \langle T_{l-1}\rangle$, linear scale. Note the initial increase.

from the 2/3 law, we found in our numerical solutions that it takes about an order of magnitude longer than a turnover time for the cascade to equilibrate. This was most apparent in simulations of the small cascade with constant largest eddy energy input, where initially the energy was contained only in level $l = 0$.

We conclude this also from the time dependence of the $E_l(t)$, as displayed in Fig. 6. There are many generations of smaller eddies within the lifetime of the largest eddy, as seen from the fine structure of $E_4(t)$. But the $E_l(t)$ may nevertheless take long ($\gg 1$) excursions from their mean values, even after the equilibrium state is reached.

In grid turbulence, the disturbances produced behind the grid are carried downstream by the mean flow, where they are allowed to decay freely.[34] So, when measuring at some distance behind the grid, one might expect to have no influence of the shear. But even if this picture is correct, the measured spectra may well depend significantly on the initial energy distribution of the disturbances, since the lifetime of one eddy turnover does not seem to allow for complete equilibration, at least in the Fourier–Weierstrass description of high turbulence, which we analyzed here. We seem to agree with the results of the "mapping closure" for the probability distribution function forwarded recently by Kraichnan.[22,35] He found μ, μ_S, μ_K, and $\delta\zeta(m)$ to vanish. There is stochastics but the cascade is no fractal or multifractal process.

After finishing this manuscript we received a recent preprint[36] in which a mode system similar to ours is introduced and treated by renormalization group methods. Again, classical scaling results within the error.

According to our simulations, for our restricted set of spatially coherent plane-wave modes there are two possible sources of exponent deviations $\delta\zeta(m)$ both of which are not really intermittency corrections. The first is additional energy input in the inertial range due to the slow decrease of the driving laminar profile's spectrum and the second is unexpectedly long equilibration times and long lasting excursions from equilibrium of the energy distribution. If both effects are controlled, our results are compatible with $\delta\zeta(m) = 0$, i.e., despite chaotic, high Re_λ turbulence, there is no intermittency effect as far as being due to temporal deterministic chaos of the hierarchy of mode amplitudes.

We recently extended the Fourier–Weierstrass mode decomposition to allow for spatial branching of the eddy decay process. Level $l = 0$ consisted of one box, the next smaller eddies $l = 1$, with half the original wavelength, consisted of $2^3 = 8$ boxes each having independent mode amplitudes, and so forth. This branching leads via Navier–Stokes interaction to a spatially statistical distribution of the transferred energy from one level to the next and affect both the moment exponents as well as the probability distribution of the velocity differences $v_i(\mathbf{r};\mathbf{x},t) = u_i(\mathbf{x}+\mathbf{r},t) - u_i(\mathbf{x},t)$. The latter $[v(r)]$ becomes (with decreasing scale r) exponential instead of Gaussian as it is in the nonbranching plane wave $\exp(i\mathbf{p}\cdot\mathbf{x})$, $\mathbf{p}\in K$, decomposition. The former ones, the moment exponents, were found to be $\zeta(2) = 0.70$, $\zeta(4) = 1.27$, $\zeta(6) = 1.70$, and $\zeta(8) = 1.94$. Details will be published separately.[37]

APPENDIX: KOLMOGOROV STRUCTURE EQUATION

We give here a short derivation of the Kolmogorov structure equation, based on our K-restricted model. By performing the $\mathbf{y}$ and the angle averages, we obtain for the longitudinal structure functions of second and third order:

$$D_{\parallel}^{(2)}(r) = \frac{2}{3} \sum_{\mathbf{p}\in K} \langle |\mathbf{u}(\mathbf{p})|^2 \rangle g_2(pr), \tag{A1}$$

$$D_{\parallel}^{(3)}(r) = 12 \sum_{\mathbf{p},\mathbf{q}\in K} \frac{p_j}{p} \times \mathrm{Im}[\langle u_i^*(\mathbf{p}) u_j(\mathbf{p}-\mathbf{q}) u_i(\mathbf{q}) \rangle] g_3(pr). \tag{A2}$$

Here, the functions g_2, g_3 are introduced, which contain the scale r and the geometry of the three-dimensional flow

$$g_2(pr) = (pr)^{-3}\{(pr)^3 + 3[pr\cos(pr) - \sin(pr)]\}, \tag{A3}$$

$$g_3(pr) = (pr)^{-4}\{[3 - (pr)^2]\sin(pr) - 3pr\cos(pr)\}. \tag{A4}$$

We now multiply (9) with $12u_i^*(\mathbf{p})p^{-1}g_3(pr)$ and take the ensemble average. In the stationary state, this gives

$$\begin{aligned} 0 = & -iM_{ijk}(\mathbf{p}) \sum_{\mathbf{q}\in K} \langle u_i^*(\mathbf{p}) u_j(\mathbf{p}-\mathbf{q}) u_l(\mathbf{q}) \rangle \\ & \times 12p^{-1}g_3(pr) - 12\nu p^2 \langle |\mathbf{u}(\mathbf{p})|^2 \rangle p^{-1} g_3(pr) \\ & + 12p^{-1}g_3(pr)\langle u_i^*(\mathbf{p}) f_i(\mathbf{p}) \rangle. \end{aligned}$$

Using

$$\sum_{\mathbf{q}\in K} -iM_{ijl}(\mathbf{p}) \langle u_i^*(\mathbf{p}) u_j(\mathbf{p}-\mathbf{q}) u_l(\mathbf{q}) \rangle = \sum_{\mathbf{q}\in K} p_j \,\mathrm{Im}[\langle u_i^*(\mathbf{p}) u_j(\mathbf{p}-\mathbf{q}) u_i(\mathbf{q}) \rangle]$$

and summing over all $\mathbf{p}\in K$ we obtain

$$\begin{aligned} 0 = & D_{\parallel}^{(3)}(r) - 6\nu\,\partial_r D_{\parallel}^{(2)}(r) \\ & + 12 \sum_{\mathbf{p}\in K} \langle u_i^*(\mathbf{p}) f_i(\mathbf{p}) \rangle p^{-1} g_3(pr). \end{aligned} \tag{A5}$$

The Kolmogorov structure equation thus depends on the form of the external force $f_i(\mathbf{p})$. In the case of the force (19), which only acts on the largest scales, one may expand $g_3(pr)$ for $r \ll L$, $p^{-1}g_3(pr) \to r/15$. This gives

$$12 \sum_{\mathbf{p}\in K} \langle u_i^*(\mathbf{p}) f_i(\mathbf{p}) \rangle p^{-1} g_3(pr) = \frac{4}{5}\epsilon r.$$

So (A5) finally leads to (22).

[1] A. S. Monin and A. M. Yaglom, *Statistical Fluid Mechanics* (MIT Press, Cambridge, MA, 1971), Vol. 2.
[2] H. Effinger and S. Grossmann, Z. Phys. B **66**, 289 (1987).
[3] A. N. Kolmogorov, C. R. Akad. Nauk USSR **30**, 299 (1941).
[4] A. M. Obukhov, C. R. Akad. Nauk USSR **32**, 19 (1941).
[5] C. F. von Weizsäcker, Z. Phys. **124**, 614 (1948).
[6] W. Heisenberg, Z. Phys. **124**, 628 (1948).
[7] L. Onsager, Phys. Rev. **68**, 286 (1945).
[8] F. Anselmet, Y. Gagne, E. J. Hopfinger, and R. A. Antonia, J. Fluid Mech. **140**, 63 (1984).
[9] L. D. Landau and E. M. Lifshitz, *Fluid Mechanics* (Pergamon, London, 1963).
[10] K. R. Sreenivasan, R. Ramshankar, and C. Meneveau, Proc. R. Soc. London Ser. A **421**, 79 (1989).
[11] R. M. Kerr, J. Fluid Mech. **153**, 31 (1985).
[12] C. W. Van Atta and R. A. Antonia, Phys. Fluids **23**, 252 (1980).
[13] H. Tennekes, Phys. Fluids **11**, 669 (1968); J. C. Wyngaard and H. Tennekes, Phys. Fluids **13**, 1962 (1970).
[14] A. N. Kolmogorov, J. Fluid Mech. **13**, 82 (1962); A. M. Obukhov, J. Fluid Mech. **13**, 77 (1962).
[15] B. B. Mandelbrot, J. Fluid Mech. **62**, 331 (1974).
[16] U. Frisch, P. L. Sulem, and M. Nelkin, J. Fluid Mech. **87**, 719 (1978).
[17] R. Benzi, G. Paladin, G. Parisi, and A. Vulpiani, J. Phys. A **17**, 3521 (1984).
[18] R. H. Kraichnan, J. Fluid Mech. **5**, 497 (1959); Phys. Fluids **8**, 575 (1965).
[19] S. A. Orszag, in *Fluid Dynamics, 1973—Les Houches Summer School of Theoretical Physics,* edited by R. Balian and J. L. Peube (Gordon and Breach, New York, 1977).
[20] F. Argoul, A. Arnéodo, G. Grasseau, Y. Gagne, E. J. Hopfinger, and U. Frisch, Nature **338**, 51 (1989).
[21] V. I. Belinicher and V. S. L'vov, Sov. Phys. JETP **66**, 303 (1987).
[22] R. H. Kraichnan, Phys. Rev. Lett. **65**, 575 (1990).
[23] A. Erzan, S. Grossmann, and A. Hernández-Machado, J. Phys. A **20**, 3913 (1987); J. Eggers and S. Grossmann, "Effect of dissipation fluctuations on anomalous velocity scaling in turbulence," preprint, Univ. Marburg, 1990.
[24] E. D. Siggia, Phys. Rev. A **15**, 1730 (1977); R. M. Kerr and E. D. Siggia, J. Stat. Phys. **19**, 543 (1978).
[25] R. M. Kerr, Cooperative thesis No. 64, NCAR, Appendix (1981).
[26] K. R. Sreenivasan and C. Meneveau, Phys. Rev. A **38**, 6287 (1988).
[27] S. Grossmann and S. Thomae, Z. Phys. B **49**, 253 (1982).
[28] C. W. Van Atta and W. Y. Chen, J. Fluid Mech. **44**, 145 (1970).
[29] G. K. Batchelor, Proc. Cambridge Philos. Soc. **47**, 359 (1951).
[30] R. H. Kraichnan, Phys. Fluids **7**, 1723 (1964).
[31] W. H. Press, B. P. Flannery, S. A. Teukolsky, and W. T. Vetterling, *Numerical Recipes* (Cambridge U.P., Cambridge, MA, 1986).
[32] J. Lee, J. Fluid Mech. **101**, 349 (1980).
[33] R. M. Kerr, J. Fluid Mech. **211**, 309 (1990).
[34] P. Bradshaw, *An Introduction to Turbulence and its Measurement* (Pergamon, Oxford, 1975).
[35] H. Chen, S. Chen, and R. H. Kraichnan, Phys. Rev. Lett. **63**, 2657 (1989).
[36] R. Blender, "Inertial range spectrum of a fractal model for turbulence," preprint, FU Berlin, 1990.
[37] J. Eggers and S. Grossmann, Phys. Lett. A (in press).